*Supporting Information*

# Conjugated Polyelectrolyte-Based Ternary Exciton Funnels via Liposome Scaffolds

Jack Palmer,[1≠] Carmen J. Segura,[1] Levi Matsushima,[1] Benjamin Abrams,[2]

Hsiau-Wei Lee,[1] Alexander L. Ayzner[1*]

[1] Department of Chemistry and Biochemistry, University of California Santa Cruz, Santa Cruz, CA, USA

[2] Life Sciences Microscopy Center, University of California Santa Cruz, Santa Cruz, CA, USA

[≠] Current address: Nanoengineering Department, University of California San Diego, San Diego, CA, USA

* Corresponding author: aayzner@ucsc.edu

## Contents

## S1. Additional Experimental Details

*Small-Angle X-ray Scattering (SAXS)*

SAXS measurements were performed at beamline 4−2 at the Stanford Synchrotron Radiation Laboratory (SSRL) using a Rayonix MX225-HE detector. The incident photon energy was 11 keV X-ray (1.17 Å), and the sample-detector distance was 2.5 m. Multiple 1-s exposures were taken and averaged prior to analysis. To avoid degradation, samples were oscillated during data collection. SasTool (SSRL) was used to convert collected 2D TIFF images to intensity vs. scattering vector length and to subtract solvent scattering (HPLC water). SAXS measurements were also performed at the Advanced Light Source (ALS, Lawrence Berkeley National Laboratory). Experiments were conducted with a 1.5 m sample-to-detector distance at 11 keV at the SIBYLS beamline. We found excellent agreement between measurements made at both synchrotron facilities.

*Steady-State Spectroscopy*

Optical density (OD) measurements were taken using a Shimadzu UV-2700 spectrophotometer at 1.0 nm increments with a 0.1 s integration time and a 2.0 nm slit width over the range of 300-850 nm. Photoluminescence (PL) measurements were taken using a Horiba Fluoromax-4 spectrofluorometer in a right-angle geometry in cuvettes with 1.0 mm pathlengths. Both emission and excitation wavelengths were scanned at 1.0 nm increments with a bandpass of 2.0 nm and integration time of 0.2 s over the desired range. Samples were first diluted for accurate

spectroscopy measurements. We found that samples were stable against dilution, and we observed no precipitation on the timescale of spectroscopic measurements.

*Confocal Laser Scanning Microscopy*

The sample (5 μL) was dropped directly onto a #1.5 coverslip and imaged immediately. Images were taken before any significant evaporation of the sample droplet occurred. Confocal images were acquired on a Leica SP5 confocal microscope using a 63x/1.4-0.6 oil immersion objective. 405 nm and 488 nm lasers were used at 20% power and signals collected between 415-435 nm (PFPI excited at 405 nm), 625-695 nm (raPTAK excited at 488 nm), and 415-600 nm (oCuPc/DOTAP samples when excited at 405 nm). Scan speed was fixed at 400 Hz and pixel size was 200 nm ± 5 nm for all images. Care was taken to ensure that all images shown in the main text and the Supporting Information were representative and not outliers.

Images were processed in ImageJ/FIJI.[1] Processing steps for all selected images included cropping, histogram adjustment, and LUT adjustment. Figure 3 of the main text received a different LUT ("fire") to emphasize the difference in intensity within each image. Composite images seen in Figures 11, S1, S5 and S10 were produced by overlaying PFPI and raPTAK emission using the "Overlay" function in FIJI.

*NMR*

NMR measurements were performed on a Bruker AVANCE III HD 500 MHz spectrometer equipped with a BBFO room temperature probe at 298K. All CPE/DOTAP samples were prepared in deuterated solvent. Proton spectra were collected using the standard Bruker pulse

program (zg30) using 64 scans and 4 prior dummy scans. 2D DOSY experiment were performed using the DOSY pulse program with longitudinal eddy current delay (LED) and bipolar gradient pulses and two spoil gradients. The diffusion-encoding pulsed field gradient pulse (δ) was 1200 us and the diffusion time (Δ) was set at 200 ms. Thirty pulsed field gradient amplitudes ranging from 1 to 47.5 G $cm^{-1}$ in equal steps of gradient were used. Each step was acquired using 256 scans. The NMR data were processed using Mestrenova.

*Time-Resolved PL Measurements*

PL lifetime measurements of samples were carried out through time correlated single photon counting (TCSPC) on a home-built laser system. Samples were excited with a supercontinuum picosecond laser (Super K EXTREME, NKT Photonics) coupled to an acousto-optic filter and an external RF driver (Super K Select, NKT Photonics). The excitation pulse was set to 430 nm and 78 MHz pulse repetition rate. The pre-sample linear polarizer (Glans-Thompson) was set to 0˚ (vertical) while the post-sample linear polarizer was set to 54.7˚ – the magic angle. Samples were analyzed in a front-faced geometry in order to minimize reflections and scattering influences from large assemblies. With detection centered around 530 nm, a 500nm long-pass filter was used on the detection arm to reduce elastic sample scattering and reflections from the sample cuvette. Emitted light was selected with a monochromator slit (Princeton Instruments, Acton Spectra Pro SP-2300) after being collimated and focused by achromatic doublets (ThorLabs). A hybrid PMT (Becker and Hickl) collected the time-resolved PL decay. The PMT feeds into an SPC-130 photon counting module (Becker and Hickl) coupled to a Simple Tau 130 TCSPC system. Measurements were carried out until approximately 10,000 counts were recorded on the main channel in order to produce robust statistics. Each

measurement reflects an average of three measurements conducted sequentially. Decay curves were deconvoluted from the instrument response functions—measured with a Ludox scattering solution—and fit to a biexponential model. Fitting of data was done using DecayFit software (Fluorescence Decay Analysis Software 1.3, FluorTools, www.fluortools.com, developed by Dr. Soren Preus) using non-linear least squares fitting minimization.

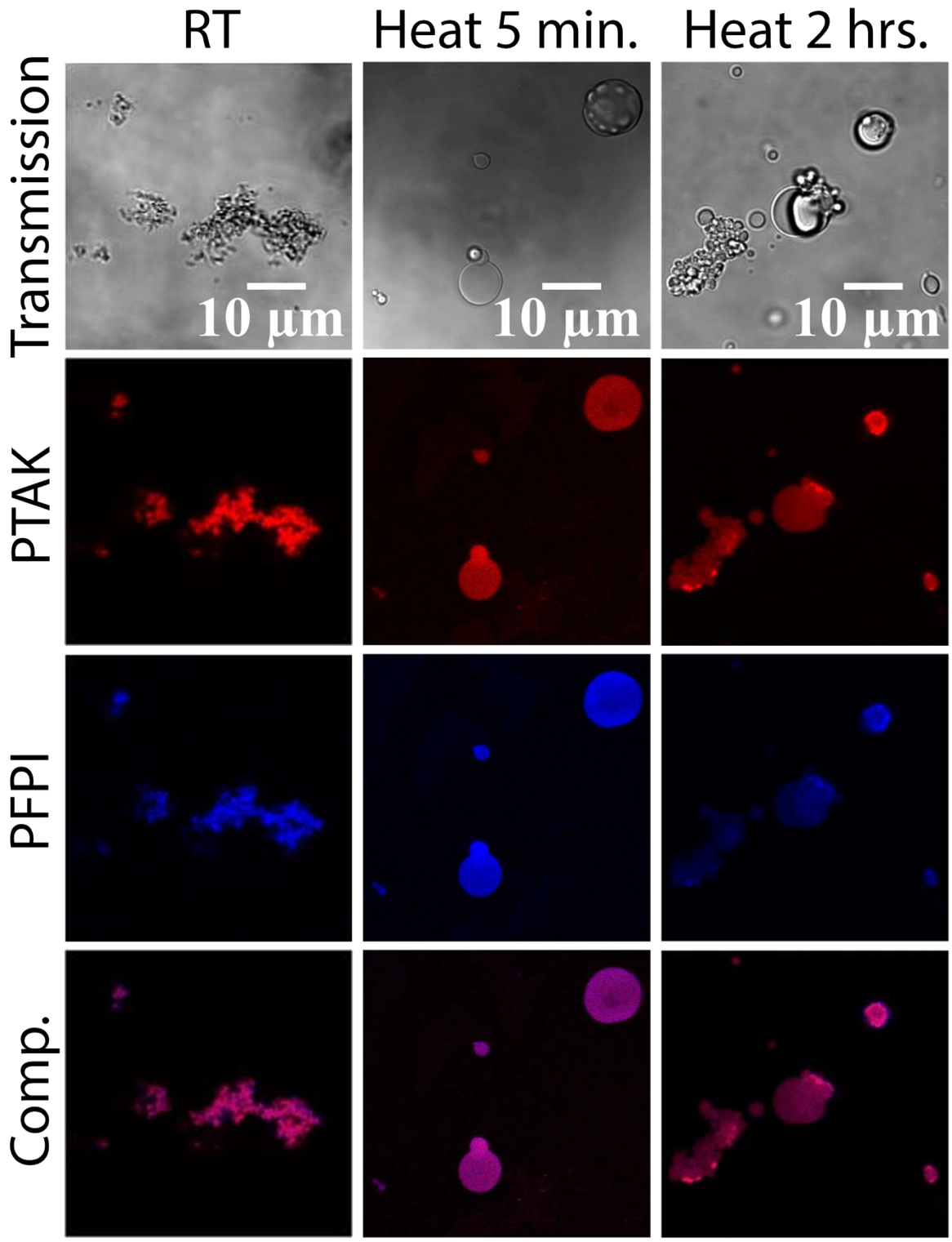


**Figure S1.** Confocal microscopy images of PFPI/raPTAK/liposome assemblies prepared by adding PFPI under different conditions (column labels). RT = room temperature. The bottom shows the composite PL image.

## S2. Effect of Preparation Conditions on PFPI/raPTAK/DOTAP Assembly Morphology

Figure S1 shows confocal microscopy images of PFPI/raPTAK/liposome assemblies prepared by adding PFPI to raPTAK-coated liposomes under the following conditions: (1) introducing PFPI at room temperature, (2) introducing PFPI at 70 ºC, and quickly cooling the sample in ice water after a 5-min heating period, and (3) heating for 2 hours at 70 ºC and slowly cooling to room temperature.

## S3. oCuPc-loaded Liposome OD

Figure S2 shows the oCuPc/DOTAP sample OD, which demonstrates that oCuPc is effectively removed when oCuPc-loaded liposomes are extruded through a 200-nm nanopore membrane.

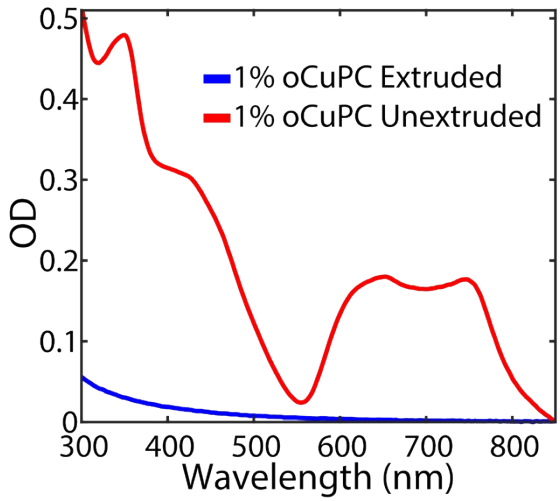


**Figure S2**. OD spectra showing the effect of the extrusion process on oCuPc-loaded liposomes.

## S4. DOSY Spectra of raPTAK/DOTAP Complexes

Since DOTAP has no proton resonances in the aromatic region, we focused on these raPTAK protons as a clean indicator of the polymer state both in isolation and after heating in the presence of DOTAP at 70˚C. Figure S3 a) shows $^{1}$H NMR spectra of pristine raPTAK chains in aqueous solution, while Figure S3 c) shows corresponding changes in intensity at varying gradient pulse strengths. Intensity in the aromatic region clearly decreases as a function of increasing gradient strength, as expected for a polymer backbone undergoing diffusive motion. In contrast, Figures S3 b) and d) show that the raPTAK aromatic signal intensity completely disappears in the presence of DOTAP liposomes after heating at 70 ºC. This loss of intensity is an indication that diffusive motion of the aromatic raPTAK backbone is highly restricted. This is consistent with raPTAK being bound to DOTAP liposomes, leading to extreme broadening of the aromatic region. The resonances around 1 ppm of Figure S3 d) are unique to DOTAP. The integrated intensities of these protons show no change at various gradient strength, which is indicative of a large molecular assembly.

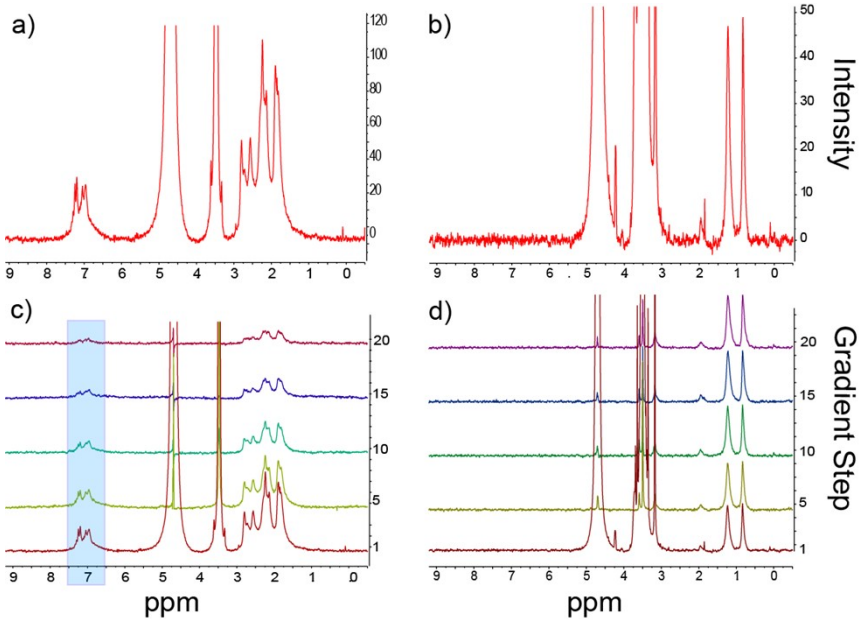


**Figure S3.** $^{1}$H NMR and corresponding DOSY spectra of (a, c) raPTAK in isolated aqueous solution, and (b, d) the raPTAK/DOTAP liposomes prepared at 70 ºC. The shaded blue box highlights the raPTAK aromatic proton region.

## S5. raPTAK/DOTAPComplex OD

We discuss in the main text that the raPTAK OD $\lambda_{max}$ undergoes a ~30 nm blueshift when bound to the liposome surface. In Figure S4, the OD of pristine raPTAK is shown in red and liposome-bound raPTAK is shown in orange. We aimed to determine whether the blueshift persisted when bound to oCuPc-impregnanted liposomes. To separate the raPTAK and oCuPc OD contributions in the raPTAK/oCuPc/liposome spectrum (pink curve), the OD of oCuPc-liposomes without raPTAK (blue curve) was subtracted off, effectively only leaving the raPTAK contribution to absorbance (grey dotted curve). A blueshift in the contribution is indeed observed, and the spectrum coincides well with the OD of liposome-bound raPTAK.

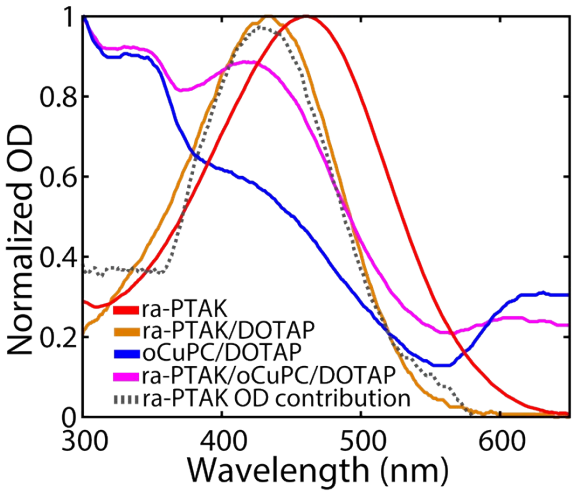


**Figure S4.** Normalized OD spectra highlighting the presence of a blueshift in the OD of raPTAK once bound to the liposome surface. This shift remains in the presence of oCuPc-embedded liposomes.

## S6. Microscopy of PFPI/raPTAK/oCuPc/DOTAP Complexes with 10% PFPI

Confocal microscopy images were also collected for PFPI/raPTAK/oCuPc:DOTAP complexes prepared with 10% PFPI. Like samples prepared with 25% PFPI, the assembly morphologies are highly asymmetric with sizes of up to tens of microns.

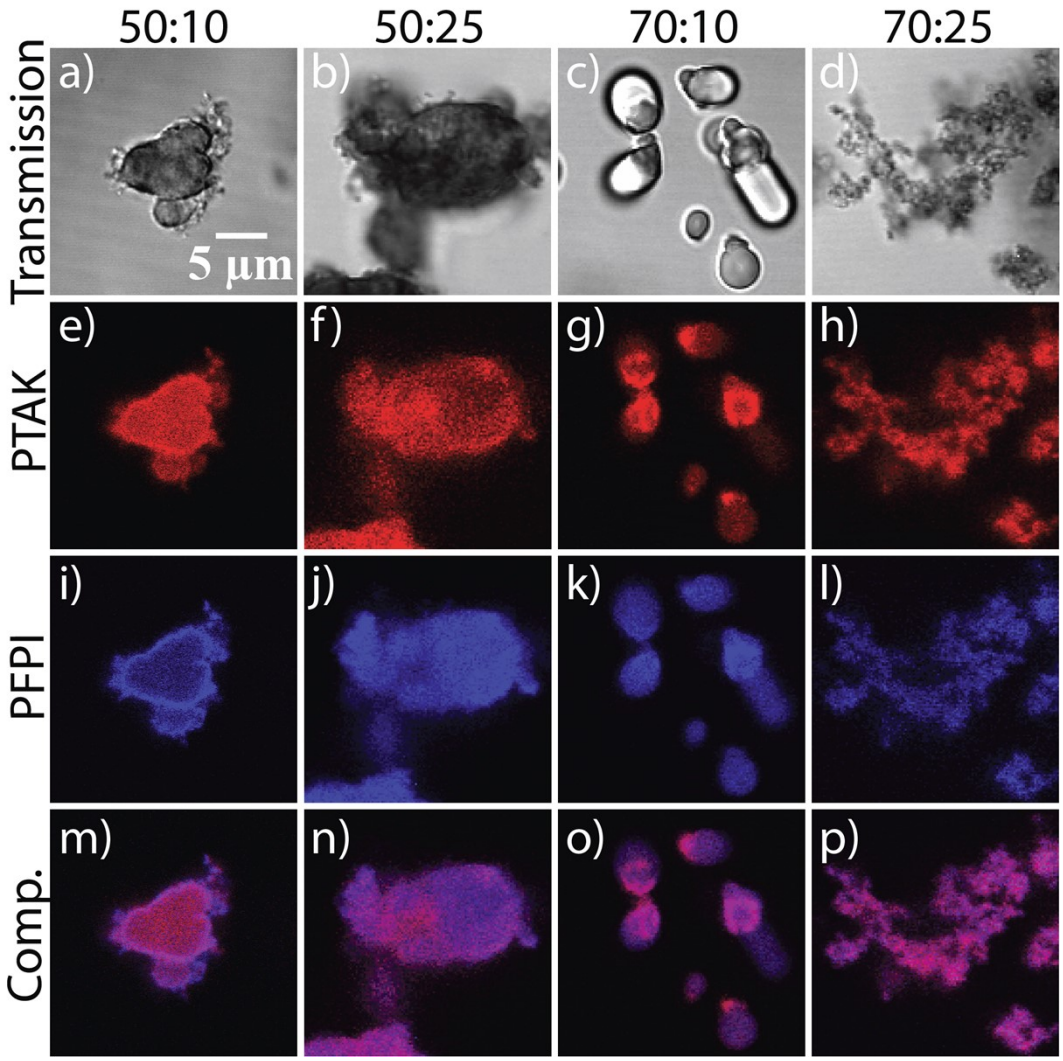


**Figure S5.** Confocal microscopy images of PFPI/raPTAK/liposome assemblies prepared by heating complexes for 5 minutes and rapidly cooling them.. The raPTAK/PFPI charge stoichiometry labels the columns. From top to bottom, the rows correspond to transmission images, PTAK PL, PFPI PL, and the composite overlay of PTAK and PFPI PL.

## S7. Quenching of PFPI PL by raPTAK

Figure S6 shows the photoluminescence spectrum of equal concentrations of PFPI with and without raPTAK present. The presence of raPTAK clearly quenches PFPI PL.

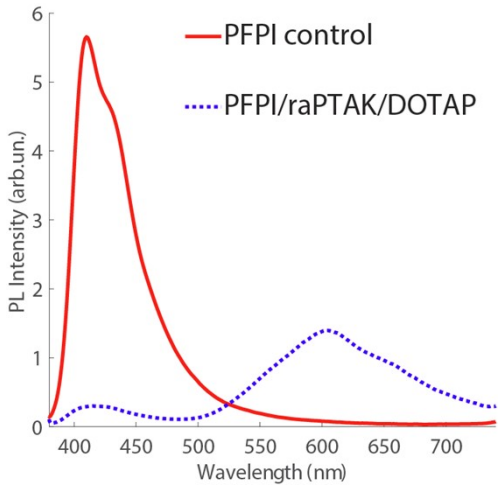


**Figure S6**. PL spectra of isolated PFPI and of PFPI/raPTAK/DOTAP complexes at the same PFPI concentration. In the complex PFPI PL is strongly quenched.

## S8. Additional Steady-State Photophysics of PFPI/raPTAK/DOTAP complexes

Figure S7 shows the OD (a), PL (b), and PLE (c) spectra of PFPI/raPTAK/liposome complexes prepared with 50% raPTAK. These samples also show an increased PLE response in the raPTAK PL region over excitation wavelengths where PFPI absorbs. As mentioned in the main text, this is strong evidence for energy transfer from PFPI to raPTAK.

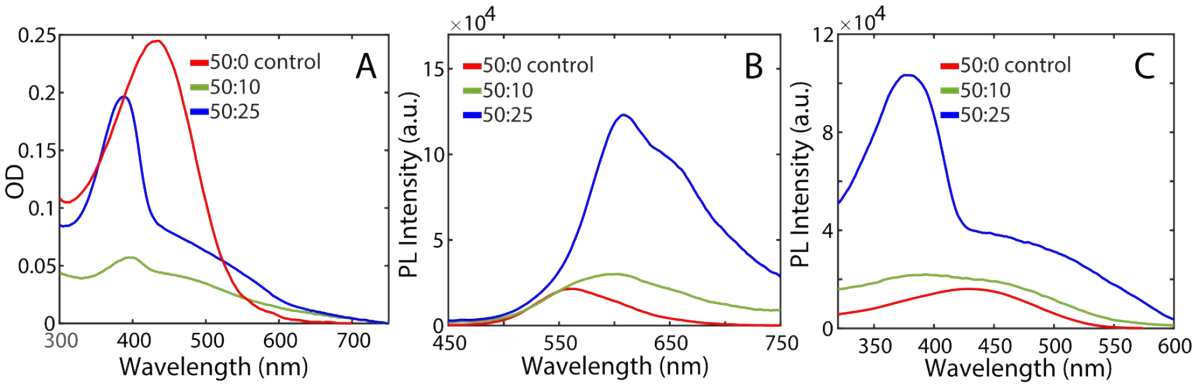


**Figure S7.** (A) OD of PFPI/raPTAK/liposomes samples prepared with 50% raPTAK, (B) PL and (C) PLE of the same sample set. For the PL spectra, samples were excited at 400 nm. For PLE, the PL wavelength was fixed at 625 nm.

## S9. Spectroscopy of PFPI/raPTAK/oCuPc:DOTAP Complexes with 10% PFPI

Spectroscopic measurements carried out for PFPI/raPTAK/oCuPc/DOTAP complexes prepared with 10% PFPI are shown in Figure S8. Figure S8a is similar to Figure S12, with the *Q*-band OD of oCuPc increasing monotonically as a function of oCuPc concentration. Figure S8b shows PL spectra when excited at 375 nm. raPTAK emission is centered around 600 nm, while residual (unquenched) PFPI emission is centered around ~415 nm. Figure S8c presents PLE spectra, which were collected with the emission wavelength fixed in the red region of raPTAK emission (650 nm). These spectra feature a pronounced contribution to emission centered around the region where PFPI absorbs (~380 nm).

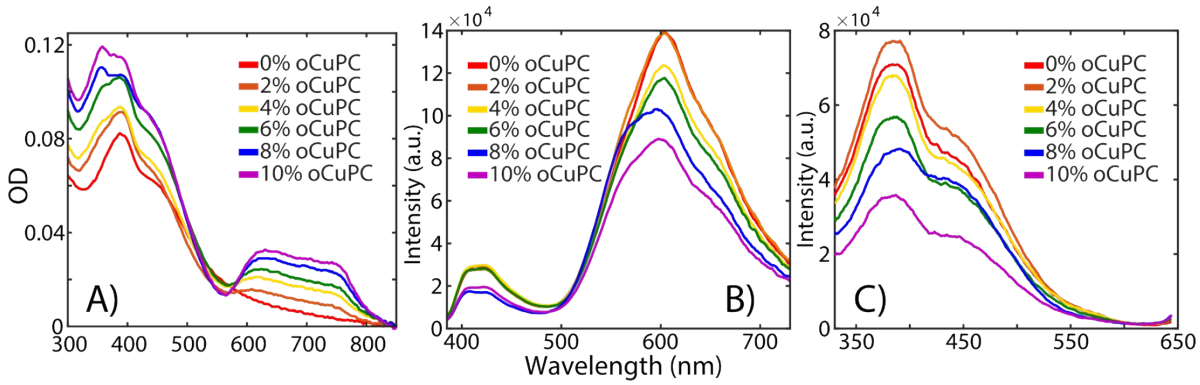


**Figure S8.** (A) OD of PFPI/raPTAK/oCuPc/liposomes samples prepared with 50% raPTAK and 10% PFPI, (B) PL and (C) PLE of the same sample set. For the PL spectra, samples were excited at 375 nm and PLE was fixed at 650 nm.

## S10. OD of PFPI/raPTAK/oCuPc:DOTAP Complexes with 25% PFPI

Figure S9 shows the OD of the PFPI/raPTAK/oCuPc:DOTAP complexes, while the inset highlights the *Q*-band absorption of oCuPc (600-800 nm). The *Q*-band OD increases monotonically as a function of oCuPc concentration in samples prepared with 50:25 raPTAK:PFPI relative molar charge ratio.

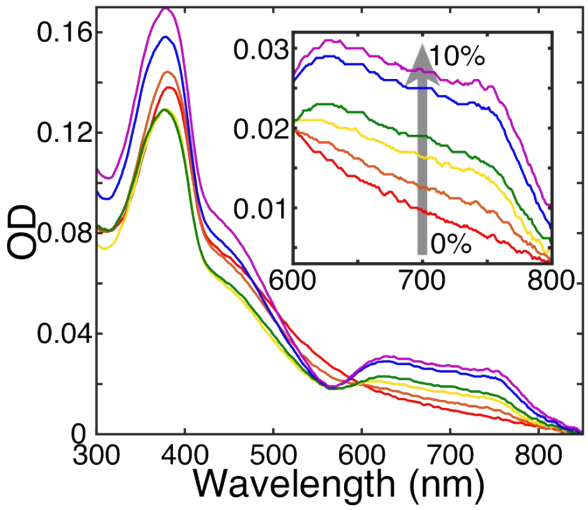


**Figure S9**. OD of PFPI/ra-PTAK/oCuPc/DOTAP samples. The inset shows increasing oCuPc OD contribution as a function of oCuPc concentration from 0 to 10% in 2% increments.

## S11. SAXS of raPTAK/DOTAP Complexes

Liposomes heated to 35 ºC (and cooled prior to measurement) show less pronounced fringes than the corresponding room-temperature sample (Figure S10a). Interestingly, Figure S10b shows that bare liposomes heated to 70 ºC show no fringes and no apparent lipid bilayer peak, implying that the liposome state has been destabilized. In contrast, liposomes covered with raPTAK continue to display the bilayer peak. As the raPTAK fraction increases, this peak progressively broadens, while simultaneously the scattering intensity increases at low Q. The latter is a hallmark of increased aggregation. Curves for 50% and 70% samples display a change in scattering intensity slope at $Q^* \sim 0.02$ Å$^{-1}$. Curves for samples with increased CPE coverage show a single linear slope of ~3 on a double-logarithmic plot at $Q < 0.05$ Å$^{-1}$ .

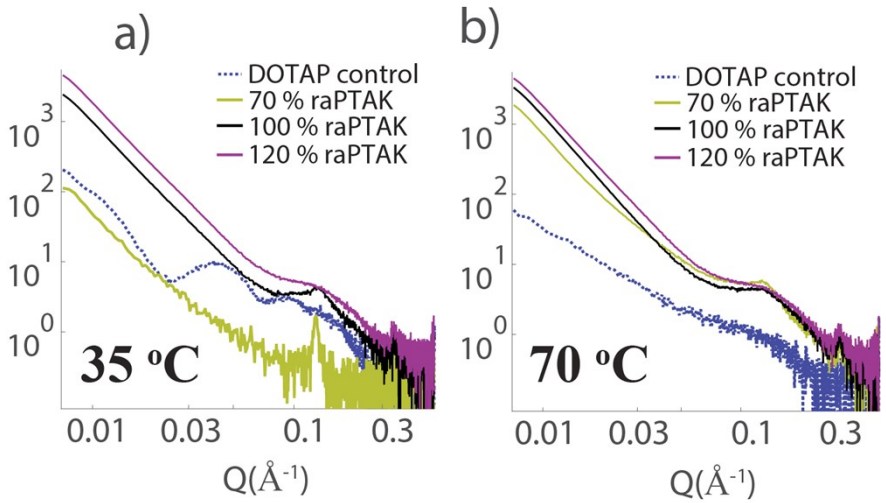


**Figure S10.** SAXS curves for raPTAK/DOTAP assemblies heated to 35°C and 70°C (panels a) and b) respectively)

## S12. SAXS of PFPI/raPTAK/DOTAP Complexes

The SAXS profiles of the raPTAK/PFPI/DOTAP complexes all show the characteristic bilayer Bragg peak centered at ~0.13Å$^{-1}$, with a d-spacing corresponding to the bilayer thickness of the liposomes. The 70:10 raPTAK:PFPI sample showed a relatively sharp peak in this region, possibly indicating a larger coherence length. This likely an indication that these samples have a higher number of multilamellar liposomes. Interestingly, there is an obvious decrease in the intensity and sharpness of the higher-Q peak, corresponding to sidechain-sidechain interactions. This indicates that the addition of PFPI partially disrupts the microstructural ordering of the raPTAK chain on the liposome surface.

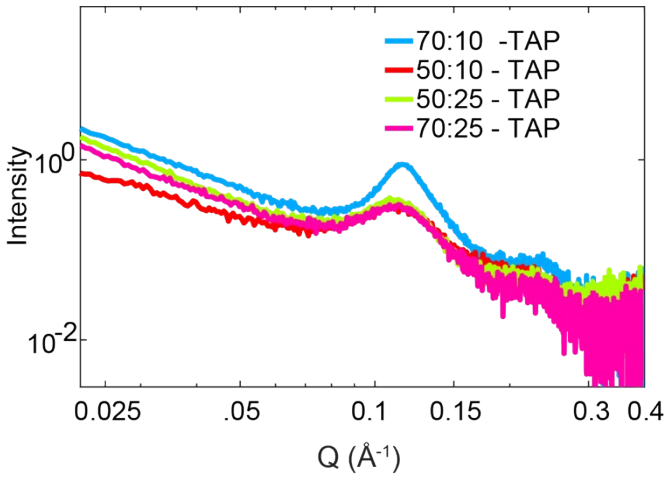


**Figure S11.** SAXS of raPTAK/PFPI/DOTAP Complexes. The legend specifies the raPTAK/PFPI molar charge ratio.

## S13. raPTAK/DOTAP Assembly Morphology: Effect of raPTAK Concentration

Having demonstrated that raPTAK/liposome complex formation is most favorable at elevated temperatures, we fixed the preparation temperature at 70 ºC and interrogated the influence of relative stoichiometry on complex structure. Figure S12 shows confocal microscopy images for a select group of charge ratios. We find that coverages below 90%, raPTAK/DOTAP liposomes appear largely spherical. At 90% (Figure S12 b and S12 e), the shape of the assembly significantly departs from sphericity and shows aggregation. This is reasonable, since for charge stoichiometries well below 100%, the assembly has a net charge. In the vicinity of charge equivalence, raPTAK/liposome complexes may be driven to aggregate due to decreased inter-particle repulsion. At 120% raPTAK we find evidence for both large spherical particles and larger particle colonies (Figure S12 c,f).

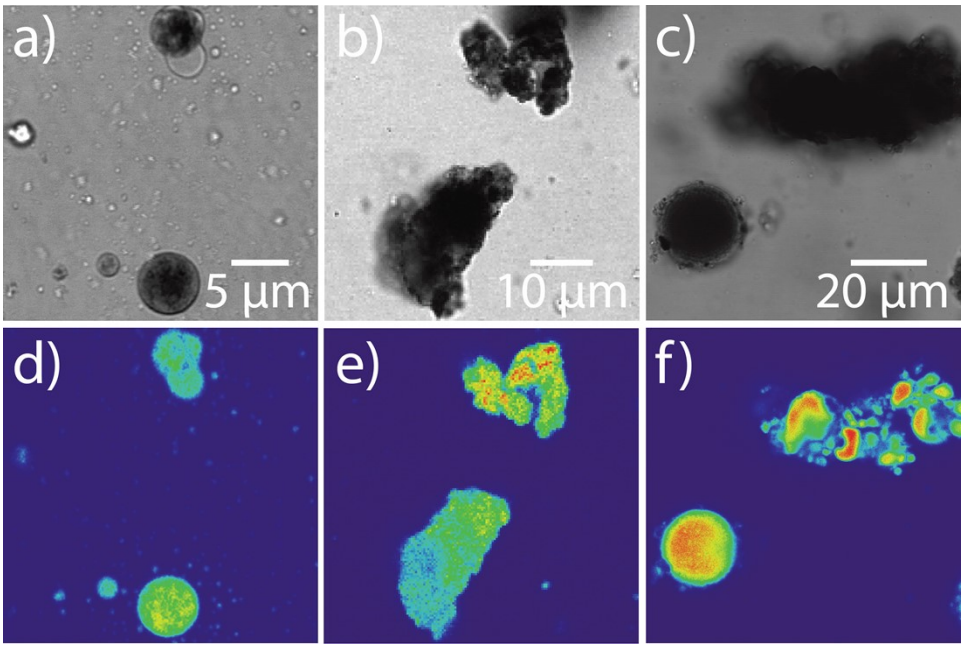


**Figure S12.** Transmission (top row) and fluorescence (bottom row) images of ra-PTAK/DOTAP samples prepared with 70%, 90%, and 120% ra-PTAK (a/d, b/e, c/f respectively).

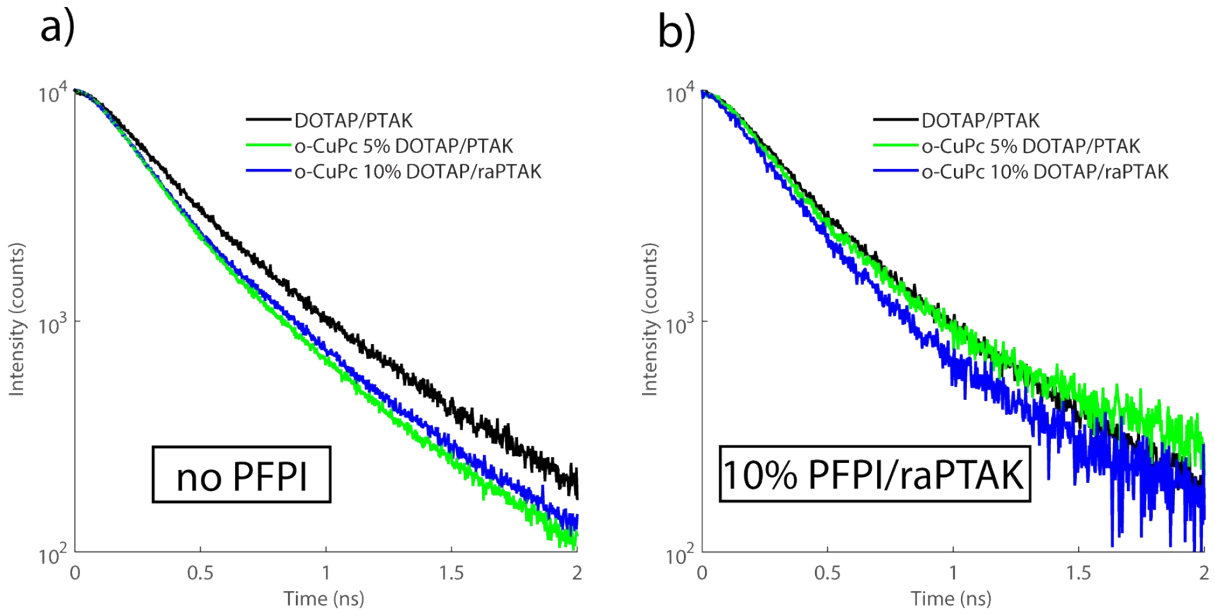


**Figure S13.** Time-resolved PL of liposome assemblies a) without PFPI, and b) with 10% PFPI charge relative to total raPTAK charge.

## S14. Time-Resolved PL Measurements

**Table S1.** Deconvolved average PL lifetimes.

| **Lifetime Components** | **<τ> (ns)** |
|---|---|
| raPTAK/DOTAP | 0.101 |
| PFPI/raPTAK/DOTAP | 0.102 |
| raPTAK/oCuPc (5%):DOTAP | 0.078 |
| PFPI/raPTAK/oCuPc (5%):DOTAP | 0.107 |
| raPTAK/oCuPc (10%):DOTAP | 0.088 |
| PFPI/raPTAK/oCuPc (10%):DOTAP | 0.092 |

## References:

1. Schindelin, J., et al., Fiji: An Open-Source Platform for Biological-Image Analysis. *Nature Methods* **2012**, *9*, 676-682.